EARTH SCIENCES
RESEARCH JOURNAL
Earth Sci. Res. J. Vol. 28, No. 2 (June, 2024): 175 - 181

UNIVERSIDAD NACIONAL DE COLOMBIA

GEOPHYSICS

Diffraction Separation for the Ground Penetrating Radar Data by Masking Filters

Zhijun Li[1,2], Hui Sun[3]*, Ruoge Xu[3], Rui Chen[3], Hongyong Ren[3], Chenglang Wang[3], Fuliu Gao[3], Mingnian Wang[1]

1. School of Civil Engineering, Southwest Jiaotong University, Chengdu, China.

2. China Railway Tunnel Group Co., Ltd., Guangzhou, China.

3. Faculty of Geosciences and Environmental Engineering, Southwest Jiaotong University, Chengdu, China.

* Corresponding author: sunhui@swjtu.edu.cn

ABSTRACT:

Ground penetrating radar is a high-resolution, efficient, non-destructive geophysical detection method. It is widely used in various application scenarios such as tunnel geological prediction and road maintenance. Ground penetrating radar data contains a variety of valid signals as well as noise. The diffracted waves of ground penetrating radar contain high-resolution small target imaging information. A critical challenge in GPR applications is how to extract diffracted waves from the wave fields. We provide a strategy to achieve this goal by applying the masking filters. Considering the complexity of the ground penetrating radar wave field and the weak energy of the diffracted waves, the median filter is first employed to suppress the linear reflections and then the f-k filter and τ-p filter are implemented to further increase the proportion of diffractions in the wave fields. Three numerical experiments are employed to test the diffraction-separation method.

Keywords: Ground Penetrating Radar (GPR), Geological Disease Survey, GPR Signal Denoising, Diffraction Separation, Masking Filter

Separación por difracción de información recolectada con georradar a través de la aplicación de filtros de máscara

RESUMEN

El georradar es un método de detección geofísica de alta resolución, eficiente, y no destructivo. Se usa ampliamente en varios escenarios, como en la predicción de túneles geológicos y en el mantenimiento de carreteras. La información del georradar contiene una variedad de señales válidas pero también ruido. Las ondas difractadas del georradar contienen información detallada de pequeños objetivos en alta resolución. Uno de los principales problemas en las aplicaciones de georradar es el cómo extraer las ondas difractadas a partir de los campos de ondas. En este artículo se presenta una estrategia para lograr este objetivo a través de aplicar filtros de máscara. Al partir de la complejidad de la onda de campo del georradar y la señal débil de las ondas difractadas, el filtro mediano se usa inicialmente para suprimir las reflecciones lineales, y luego se implementan los filtros f-k y τ-p para incrementar la proporción de difracción en los campos de ondas. Se emplearon además tres experimentos numéricos para evaluar el método de separación por difracción.

Palabras clave: Georradar; detección de problemas geológicos; eliminación de ruido de señal en georradar; separación por difracción; filtros de máscara.

Record
Manuscript received: 13/02/2024
Accepted for publication: 26/07/2024

How to cite this item:
Li, Z., Sun, H., Xu, R., Chen, R., Ren, H., Wang, C., Gao, F., & Wang, M. (2024). Diffraction Separation for the Ground Penetrating Radar Data by Masking Filters. *Earth Sciences Research Journal, 28*(2), 175-181. https://doi.org/10.15446/esrj.v28n2.112936

ISSN 1794-6190 e-ISSN 2339-3459
https://doi.org/10.15446/esrj.v28n2.112936

1. Introduction

As an important applied geophysical method, ground penetrating radar (GPR) is highly efficient, user-friendly, non-invasive and widely used in tunnel geological prediction and maintenance of transportation facilities (shown in Fig. 1) (Feng et al., 2015; Zhao et al., 2018; Giovanneschi et al., 2019). The GPR data contains many different types of wave fields. The nature of these wave fields is different. The diffraction energy is weaker than the reflection energy, however, it contains many field information of small-scale geological bodies and can be used for high-resolution imaging and identification. The processing methods for diffracted waves are currently mainly focused on seismic wave processing rather than electromagnetic wave processing. Many seismic wave processing methods can be used to process GPR data (Zong et al., 2020; Yang et al., 2020; Li et al., 2021; Zong et al., 2023). Zhao et al. (2019) integrated the GPR diffraction wave separation method with the artificial intelligence method. Li and Zhang (2021) extrated the diffracted waves in Yutu-2 Rover's Lunar Penetrating Radar Data. Lin et al. (2022) enhanced optimum rank-reduction approach for achieving efficient diffraction separation. Sun et al. (2023) combined the time-frequency analysis method with inversion algorithm and applied it to road detection. The time-frequency analysis method can also be applied to GPR data processing. Lin et al. (2023) imaged the discontinuities by applying the angle gathers.

At present, there are few researches on GPR diffraction separation methods, and they mainly focus on using a single method to process the diffraction data. Using a single filter to separate them is difficult to get good results. The masking filters are implemented in the median filter, the f-k filter and the τ-p filter to extract the diffractions in this paper.

Median filtering method is a non-linear filtering technology, which has the characteristics of suppressing noise and edge protection ability. Brownrigg (1984) proposed a weighted filter to improve the median filter's processing ability. Sun and Neuvo (1994) applied the detail-preserving median in image processing according to the local measurements of impulses. Wang and Lin (1997) modified the standard median filter algorithm to remove impulsive noise efficiently. Zhou and Zhang (1999) employed the progressive switching median filter to eliminate impulsive noise from severely distorted pictures. Zhu et al. (2004) applied the median filter to remove the linear noise in the seismic data processing. Cai et al. (2006) employed the median filter for reducing random seismic noise. Dong and Xu (2007) provided a directional-weighted median filter to eliminate random impulse noise. Huo et al. (2012) introduced a new multidirectional vector filter (MD-VMF) for separating mixed seismic shot sets. This method extends the traditional median filter from scalar to vector implementation; Kang et al. (2013) proposed a new median filter forensics technology based on the statistical characteristic analysis of median filter residual (MFR); Storath and Weinmann (2018) proposed a fast algorithm for filtering signals and images based on arc distance median according to the principle of median filtering, it is verified that the efficiency of the algorithm is higher than that of the classical median filter and has good adaptability to different data; Erkan et al. (2020) presented an adaptive-frequency median filter to solve the denoising problem.

F-K filtering method is based on two-dimensional Fourier transform and is a commonly used signal denoising technology. Canales (1984) proposed a technique to mitigate stochastic interference of the seismic data. Stone (1987) proposed a spatially variable f-k filtering method based on the "ROLL-ALONG" 2-D Fourier transform, which improved the computational efficiency of the algorithm. Duncan and Beresford (1994) designed the slowness adaptive f-k filter of pre-stack seismic data. Paulus and Mars (2006) proposed a method for multicomponent or multidimensional data based on single component seismic method (F-K filter), which is applied to separate interference wave fields. Cai et al. (2011) presented a new adaptive f-k filter for the defect of poor adaptability of f-x domain denoising in complex geological structures. This method considers the time-frequency characteristics of local data, is easy to implement, and can effectively suppress random and coherent noise in complex geological structures; Chen and Jin (2015) presented a novel approach to eliminate random noise and improved seismic data resolution through the simple FK threshold step in the shaping regularization framework; Maman Herman et al. (2017) applied F-K filtering in shallow sea seismic exploration to eliminate noise in high-frequency seismic data and achieved good results; Lowney et al. (2020) designed a spatial variable filter based on plane wave destruction in f-k domain. In this method, the synthetic data and real data are used to verify the method, which proves the advantages of diffraction imaging in seismic interpretation.

τ-p filtering method is also a widely used filtering method. Radon transform theory was proposed by the famous Austrian mathematician Radon in 1917 to deal with the problem of image reconstruction (Radon, 1986); Carswell et al. (1984) applied the τ-p transform to the separation of the up and down waves of VSP seismic data, and achieved good results. The Radon transform was calculated using the least squares approach, which was examined by Thorson and Claerbout (1985). Sacchi and Ulryc (1995) proposed the high-resolution Radon transform for channel interpolation and VSP wavefield separation and achieved good application effect; Trad et al. (2003) proposed a hybrid Radon transform method for suppressing surface waves, and achieved good results. Moldoveanu-Constantinescu and Sacchi (2005) proposed a phase shift hyperbolic equation, it can be clearly seen from the results that the equation improves the resolution in the Radon transform domain. Nowak and Imhof (2006) proposed the weighted Radon transform to suppresses multiple, which can keep the transformed amplitude well; Jiang et al. (2015) applied the frequency domain high resolution Radon to the separation of P-P and P-SV waves, and the application effect was good; Gholami (2017) proposed the convolutional Radon transform, which improves the time, slowness and curvature resolution of seismic data compared with the traditional Radon transform. Andersson and Robertsson (2019) proposed a simple, fast and more accurate algorithm based on Radon transform and opposite transform, this method reduces the computational complexity and the calculated cost.

In this paper, the τ - p masking filters are applied to separate the GPR diffractions. Three filtering methods, namely the median filter, the f-k filter and the filter, are used to process different types of the high-frequency electromagnetic-wave signals and noises in GPR data. Then the purpose of extracting diffraction waves in GPR data is achieved. In the following sections, the principle of the masking filter and the principles of the filtering methods employed in it will be introduced first. Then zigzag model data, inclined layer model data and complex model data will be used to test the method in this article.

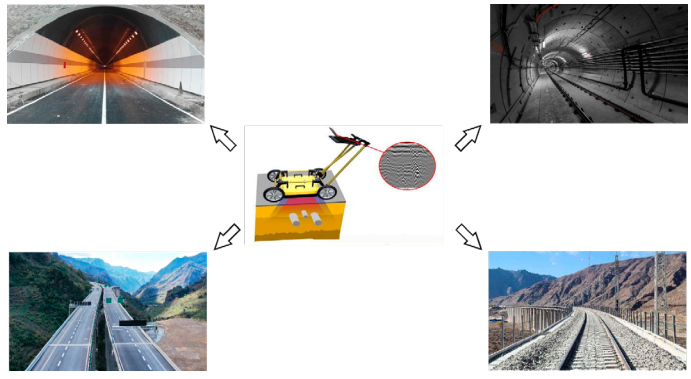

Figure 1. Application of GPR in tunnel prediction and maintenance of subways, highways and high-speed railways.

2. Method

2.1 Median filtering principle

Assume that the GPR record is described by Formula 1:

$$\left\{x_{i,j}\right\},\left(i=1,\ldots,N_x;\,j=1,\ldots,N_t\right) \tag{1}$$

Where i and j are the spatial and temporal subscripts of the data N_x is the number of spatial samples of the data, that is, the number of seismic traces; N_t is the number of time samples per seismic record. Set the data sequence of channel i be X_j (j = 1,..., Nt) , if the given median filter span is N (generally N is odd), then the median filtering process for point k of channel i data is:

1. N sample points centered on point k;
2. rank the N sample points from small to large;
3. Take the value of the center position of the ordered N sample points as the output value of point k.

Raw Data $X_{k-(N-1)/2},\ldots,X_k,\ldots,X_{k+(N+1)/2}$

Sort Data $Y_{k-(N-1)/2},\ldots,Y_k,\ldots,Y_{k+(N+1)/2}$

Output Data Y_k

Repeat the above process to realize the median filtering of seismic data record $\{x_{i,j}\}$.

The neutral filtering in phase elimination method is to subtract the filtered record Y_k from the original record X_k to obtain the result Z_k, as Formula 2:

$$Z_k = X_k - Y_k \tag{2}$$

It is sometimes referred to as subtraction median filtering.

2.2 F-K filtering principle

The F-K filtering method uses two-dimensional Fourier Transform to transform the signal in time-space domain (*x, t*) into frequency wavenumber domain (*f, k*). Let *f*(*x, t*) be about two-dimensional seismic data in time-space domain *f*(*x, t*) and contain valid signal *s*(*x, t*) and interference noise *n*(*x, t*), i.e. Formula 3:

$$(f, k) = s(x, t) + n(x, t) \tag{3}$$

Two-dimensional Fourier Transform of formula (3), i.e. Formula 4:

$$\begin{aligned}&\int_{-\infty}^{\infty}\int_{-\infty}^{\infty} f(x,t)e^{-j(2\pi ft+2\pi kx)}dxdt\\&=\int_{-\infty}^{\infty}\int_{-\infty}^{\infty} s(x,t)e^{-j(2\pi ft+2\pi kx)}dxdt\\&+\int_{-\infty}^{\infty}\int_{-\infty}^{\infty} n(x,t)e^{-j(2\pi ft+2\pi kx)}dxdt\end{aligned} \tag{4}$$

This shifts the signal from domain (*x,t*) to domain (*f,x*), *f* to frequency and *k* to wavenumber. The formula above is simplified to Formula 5:

$$F(f,x) = S(f,x) + N(f,x) \tag{5}$$

Where $F(f,x)$ is the frequency wavenumber spectrum of the original two-dimensional signal *f*(*x, t*); *S*(*f, k*) is the frequency wavenumber spectrum of the effective signal *s*(*x, t*) and *N*(*f, k*) is the frequency wavenumber spectrum of the interference noise *n*(*x, t*).

F-K filtering refers to the filtering in frequency-wavenumber domain for signals in time-space domain (*x,t*). The designed filtering factor is a function of time-space *H*(*f,k*).The filtering process is a product process in frequency-wavenumber domain. The specific process is as follows:

In area (*f,k*), a two-dimensional filter *H*(*f,k*), is designed so that in area D, as Formula 6:

$$H(f,k) = \begin{cases} 1, (f,k) \in D \\ 0, (f,k) \notin D \end{cases} \tag{6}$$

Filter *F*(*f,k*) signal through the wave, as Formula 7:

$$\hat{F}(f,k) = H(f,k)F(f,k) = \begin{cases} F(f,k) & (f,k) \in D \\ 0 & (f,k) \notin D \end{cases} \tag{7}$$

Where $\hat{F}(f,k) = \hat{S}(f,k) + \hat{N}(f,k)$ satisfies Formula 8:

$$\begin{cases} \hat{S}(f,k) = 0, (f,k) \notin D \\ \hat{N}(f,k) = 0, (f,k) \in D \end{cases} \tag{8}$$

Then the inverse Fourier transform of K in $\hat{F}(f,k)$ region is obtained Formula 9:

$$\hat{f}(f,k) = \hat{s}(f,k) + \hat{n}(f,k) \tag{9}$$

Because in area D, $N(f, k) = 0$, so we can obtain Formula 10:

$$\hat{f}(f,k) = s(x,t) \tag{10}$$

Where $\hat{f}(f,k)$ is the filtered frequency-wavenumber spectrum of the original two-dimensional signal *f*(*x, t*); $\hat{S}(f,k)$ is the filtered frequency-wavenumber spectrum of the effective signal *S*(*x, t*) and $\hat{N}(f,k)$ is the filtered frequency-wavenumber spectrum of the interference noise *n*(*x, t*).

3. Basic principle of Radon transform

In multi-wave and multi-component seismic exploration, longitudinal and transverse waves are usually mixed together, which is not conducive to observation and processing. Better separation of longitudinal and transverse waves can reduce the difficulty of data processing, improve the accuracy of inversion, and better explain the structure of underground media. Radon transform provides a way to project the data in the time domain into the Radon domain, and then transform the data of Radon domain into the time domain. The purpose of the former is to separate the components in the Radon field and eliminate the unwanted components, and the target of the latter is to retain the required waves. The result of the Radon transform clearly shows that the noise has been effectively suppressed and eliminated.

Linear Radon transform is also called tilt stack or τ - p transform. Its idea is to superimpose and sum continuous signals in the time-space domain along a straight line with slope p and intercept τ (along a certain ray path), and apply τ and to describe the trajectory of the wave.

The expressions for *d*(*t,x*) and τ - p transform are as follows Formulas 11-12:

$$m(\tau, p) = \int_{-\infty}^{\infty} d(t = \tau + px, x)\mathrm{d}x \tag{11}$$

$$d(t, x) = \int_{-\infty}^{\infty} m(\tau = t - px, p)\mathrm{d}p \tag{12}$$

Where *d*(*t,x*) is a two-dimensional continuous signal; t means two-way time; x is the offset; m(τ, p) represents the oblique superimposed signal τ; is the intercept time; $p = \dfrac{dt}{dx}$ is slowness.

Seismic records in the time-space domain are discrete samples of the signal *d*(*nt*, *nx*). When wavefield separation is performed, it is necessary to discretize formulas (11) and (12). The equations are as follows Formulas 13-14:

$$m(\tau_i, p_j) = \sum_{k=1}^{nx} d(\tau_i + p_j x_k, x_k) \tag{13}$$

$$d(t_m, x_n) = \sum_{k=1}^{np} m(t_m - p_k x_n, p_k) \tag{14}$$

Parabolic Radon transformation principle Change the integral path $t = \tau + px$ in the linear Radon transform oblique superposition formula to $t = \tau + qx^2$, so the integral path changes from a ray to a parabola. The positive and negative transformation formulas are as follows Formulas 15-16:

$$m(\tau, q) = \int_{-\infty}^{\infty} d(t = \tau + qx^2, x)\mathrm{d}x \tag{15}$$

$$d(t, x) = \int_{-\infty}^{\infty} m(\tau = t - qx^2, p)\mathrm{d}q \tag{16}$$

The processing of seismic data requires discretization, as follows Formulas 17-18:

$$m(\tau_i, p_j) = \sum_{k=1}^{nx} d(\tau_i + q_j x_k^2, x_k) \tag{17}$$

$$d(t_m, x_n) = \sum_{k=1}^{np} m\left(t_m - q_k x_n^2, q_k\right) \tag{18}$$

The schematic diagram of the diffraction-separating method using the masking filters is shown in Figure 2.

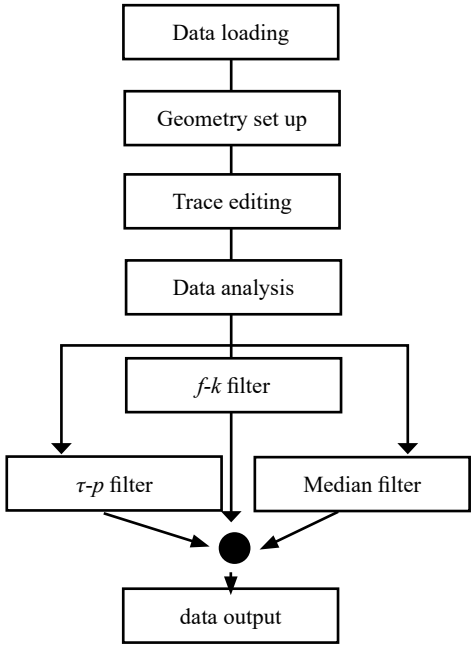

Figure 2. The flow chart of separating the diffractions using the masking filters.

4. Numerical test on a zigzag model

The first test was conducted on a zigzag model with the dielectric permittivity distribution shown in Figure 3. The model has a size of 111 × 201; The horizontal and vertical grid spacing of the model are both 0.1 m; The uppermost layer is the air layer with a dielectric constant of 1.0; The dielectric constants of the second and third layers are 9.0 and 16.0, respectively; The model contains two sharp points, which will produce diffraction hyperbolas during forward modeling. The zigzag model's GPR modeling result is displayed in Figure 4. The source's lateral location is dispersed between 0.0 and 19.7 meters, with a source interval of 0.1 meters. The offset between the source and the receiver is 0.3 meters. We can clearly see diffracted, direct, and reflected waves in Figure 4. The energy of the diffracted wave is significantly less than that of the reflected and direct waves.

Figure 5 and Figure 6 show the diffracted waves and residual wave fields obtained using masking filters, respectively. It is evident that the diffractions may be successfully extracted using the masking filter approach. However, there are still some other waves in the extraction results that are difficult to eliminate and the removed wave energy contains some diffracted waves.

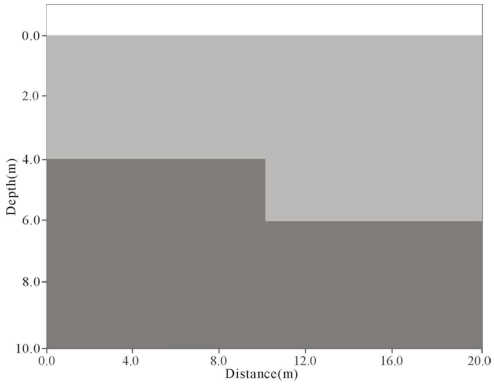

Figure 3. The dielectric permittivity distribution diagram of the zigzag model.

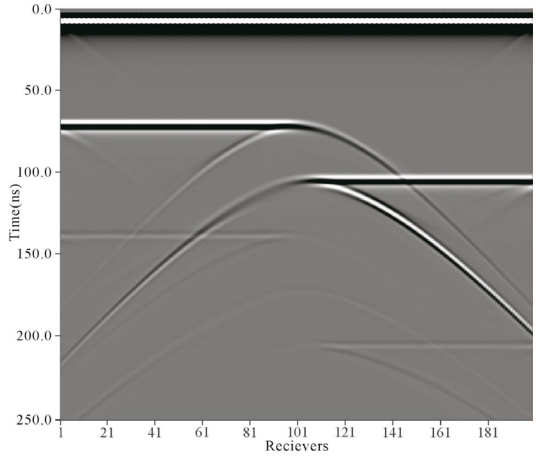

Figure 4. The GPR modeling result of the zigzag model.

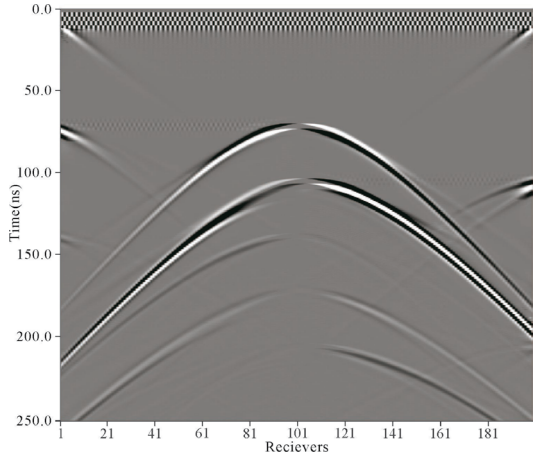

Figure 5. The diffraction separation result of the zigzag model using the masking filters.

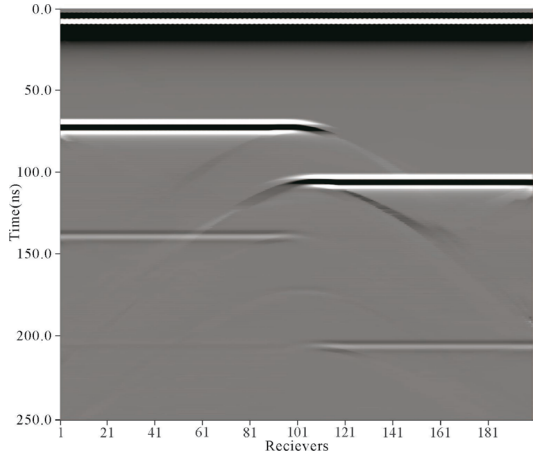

Figure 6. The residual wave fields of the zigzag model after extracting the diffractions.

5. Numerical test on an inclined layer model

The second test was performed on an inclined layer model, and the inclined layer model's dielectric constant distribution is displayed in Figure 7. Its size is 110 × 200; The horizontal and vertical grid spacing of the model is 1 m, and the dielectric constants from the first layer to the third layer are 1.0, 9.0

and 25.0, respectively. The model consists of six regularly inclined scattering points and two square anomaly blocks. The dielectric constant of the scattering points and square anomaly blocks is 16.0. Figure 8 shows the GPR forward modeling result of the inclined layer model. The sources are laterally distributed in the range of 0.0 m to19.7 m, and the source spacing is 0.1 m; From Figure 8, we can clearly see reflected wave, direct wave and diffracted wave where the diffracted wave's energy is significantly less than the energy of the reflected and direct waves.

Figure 9 and Figure 10 show diffracted waves and residual wave fields of complex models obtained using masking filters, respectively. The mask filter can effectively separate diffracted waves, and the diffraction energy is very small in the residual wave field.

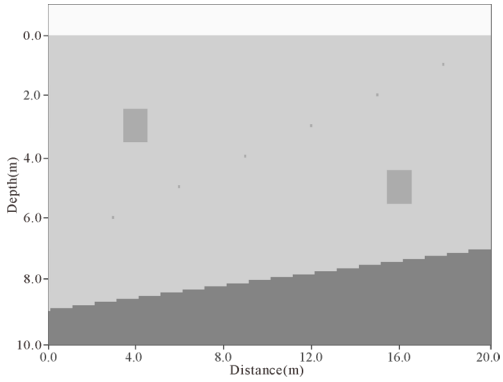

Figure 7. Dielectric constant distribution of inclined layer model.

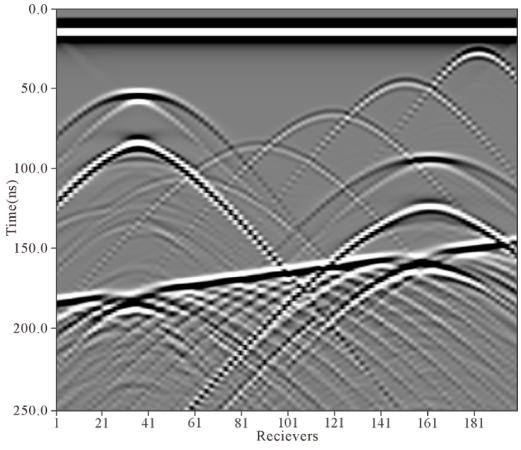

Figure 8. GPR forward modeling record of complex synthetic model.

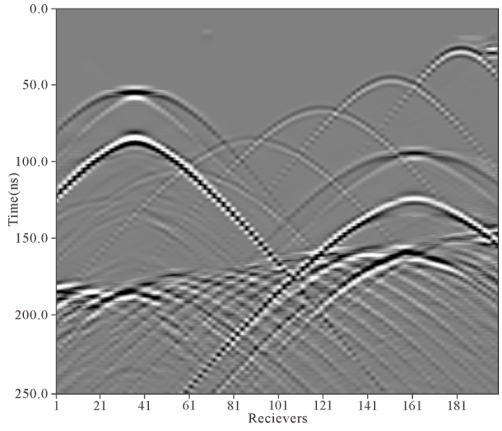

Figure 9. The diffraction separation result of the inclined layer model using the masking filters.

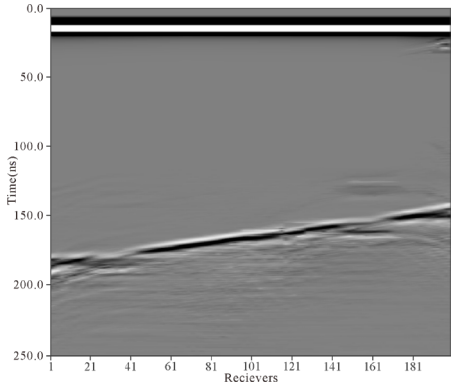

Figure 10. The residual wave fields of the inclined layer model after extracting the diffractions.

6. Numerical test on a complex model

The third test was run using a complex model. The model's dielectric permittivity distribution is displayed in Figure 11. It has a size of 400 × 800. The horizontal and vertical grid spacing of the model are both 0.05 m. From the first layer to the fourth layer, the dielectric constants are 1.0, 3.0, 4.0, 5.0. The model contains multiple scattering points and a long-strip anomaly. The scattering points and the long-strip anomaly is 0.5 larger than the stratum containing it. The complex model's modeling result is displayed in Figure 12. There is a 0.5 m source interval. The receiver and source are offset by 0.3 meters. The scattering points produce many diffracted waves in the forward result.

Figure 13 and Figure 14 show the diffracted waves and residual wave fields of the complex model obtained using masking filters, respectively. The masking filters can separate the diffracted waves well and the residual wavefields contain little diffraction energy.

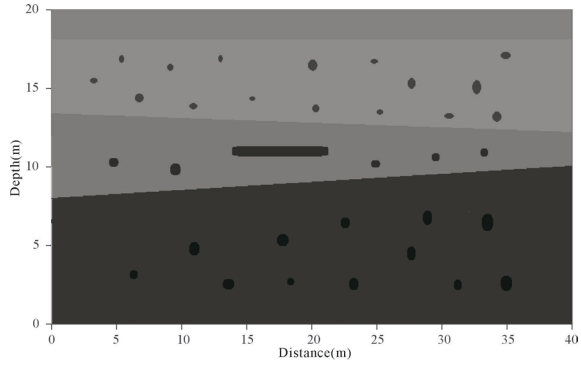

Figure 11. The dielectric permittivity distribution diagram of the complex model.

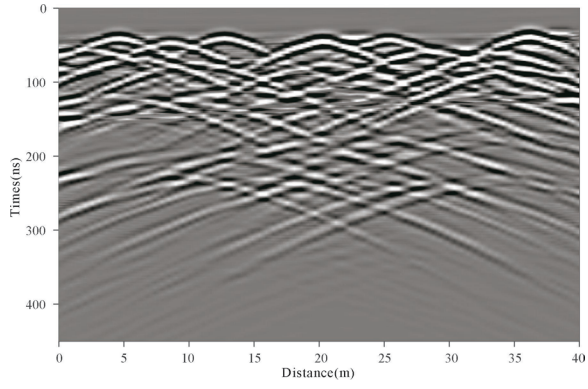

Figure 12. The diffraction separation result of the complex model using the masking filters.

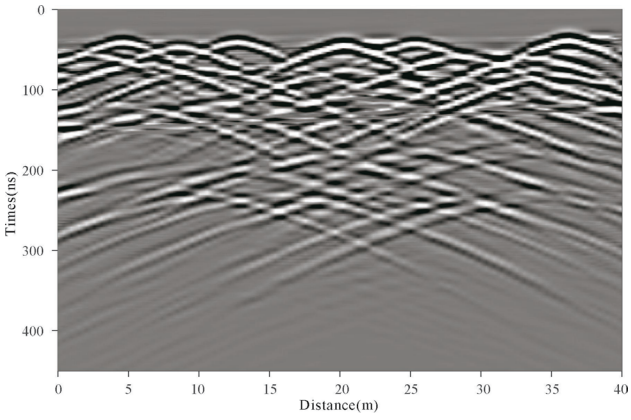

Figure 13. The diffraction separation result of the zigzag model using the masking filters.

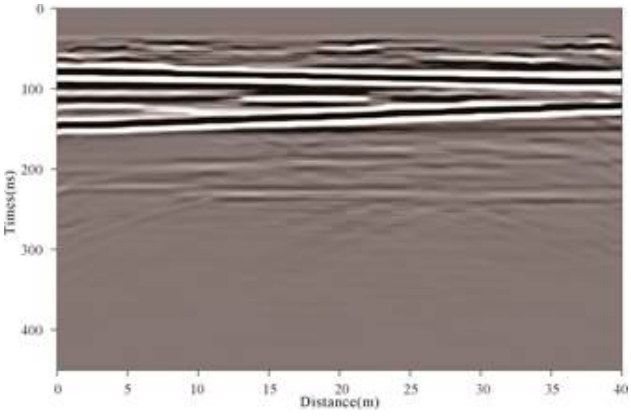

Figure 14. The residual wave fields of the complex model after extracting the diffractions.

7. Conclusion

This paper focuses on extracting the diffractions from the GPR wave fields. The masking filters are employed to finish the task. Considering the complexity of the GPR wave field, median filtering, f-k filtering and *f-p* filtering are comprehensively applied to the separation of diffracted waves. Numerical results show that these three methods can overcome their shortcomings to a certain extent, and can suppress direct waves, reflected waves and random noises to obtain good diffractions. The masking filer method can be an effective tool for diffracted wave separation.

Acknowledgment

This work was supported in part by the National Natural Science Foundation of China under Grant 42374166, in part by the Natural Science Foundation of Sichuan Province under Grant 2023NSFSC0770, and in part by the Fundamental Research Funds for the Central Universities under Grant 2682022ZTPY002 and Grant 2682022ZTPY088.

References

Andersson, F., & Robertsson, J. (2019). Fast τ-p transforms by chirp modulation. *Geophysics,* 84(1), A13-A17. https://doi.org/10.1190/geo2018-0380.1

Brownrigg, D. R. K. (1984). The weighted median filter. *Communications of the ACM,* 27(8), 807-818. https://doi.org/10.1145/358198.358222

Cai, H. P., He, Z. H., & Huang, D. J. (2011). Seismic data denoising based on mixed time-frequency methods. Applied Geophysics, 8(4), 319-327. https://doi.org/10.1007/s11770-011-0300-6

Cai, L., Yang, L., Yang, B., & Sun, J. (2006). A 2D multistage median filter to reduce random seismic noise. *Geophysics,* 71(5), V105-V110. https://doi.org/10.1190/1.2236003

Canales, L. L. (1984). Random noise reduction. *SEG Technical Program Expanded Abstracts,* 329-329. https://doi.org/10.1190/1.1894168

Carswell, A., Tang, R., Dillistone, C., & Moon, W. (1984). A new method of field separation in VSP Data Processing. *SEG Technical Program Expanded Abstracts,* 3(1), 856. https://doi.org/10.1190/1.1893982

Chen, Y. K., & Jin, Z. Y. (2015). Simultaneously removing noise and increasing resolution of seismic data using waveform shaping. *IEEE Geoscience and Remote Sensing Letters,* 13(1), 102-104. https://doi.org/10.1109/LGRS.2015.2499166

Dong, Y., & Xu, S. (2007). A new directional weighted median filter for removal of random-valued impulse noise. *IEEE Signal Processing Letters,* 14, 193-196. DOI: 10.1109/LSP.2006.884014

Duncan, G., & Berestord, G. (1994). Slowness adaptive f-k filtering of prestack seismic data. *Geophysics,* 59(1), 140-147. https://doi.org/10.1190/1.1443525

Erkan, U., Enginoğlu, S., Thanh, N. H., & Hieu, L. M. (2020). Adaptive frequency median filter for the salt and pepper denoising problem. *IET Image Processing,* 14(7), 1291-1302. https://doi.org/10.1049/iet-ipr.2019.0398

Feng, X., Yu, Y., Liu, C., & Fehler, M. (2015). Combination of H-alpha decomposition and migration for enhancing subsurface target classification of GPR. *IEEE Transactions on Geoscience and Remote Sensing,* 53(9), 4852-4861. DOI: 10.1109/TGRS.2015.2411572

Gholami, A. (2017). Deconvolutive Radon transform. *Geophysics,* 82(2), V117-V125. https://doi.org/10.1190/geo2016-0377.1

Giovanneschi, F., Mishra, K. V., Gonzalez-Huici, M. A., Eldar, Y. C., & Ender, J. H. G. (2019). Dictionary learning for adaptive GPR landmine classification. *IEEE Transactions on Geoscience and Remote Sensing,* 57(12), 10036-10055. https://doi.org/10.1109/TGRS.2019.2931134

Herman, M., Hashim, H. S., Latif, A. A., & Ghosh, D. P. (2017). Application of FK filtering for coherent noise removal in high frequency shallow marine data. IOP Conference Series: Earth and Environmental Science, 88(1), 012010. DOI: 10.1088/1755-1315/88/1/012010

Huo, S. D., Luo, Y., & Kelamis, P. G. (2012). Simultaneous sources separation via multidirectional vector-median filtering. *Geophysics,* 77(4), V123-V131. https://doi.org/10.1190/geo2011-0254.1

Jiang, X., Lin, J., Ye, F., & Zheng, F. (2015). Separation of P–P and P–SV wavefields by high resolution parabolic Radon transform. *Journal of Applied Geophysics,* 119, 192-201. https://doi.org/10.1016/j.jappgeo.2015.05.011

Kang, X. G., Stamm, M. C., Peng, A. J., & Liu, K. J. R. (2013). Robust median filtering forensics using an autoregressive model. IEEE Transactions on Information Forensics and Security, 8(9), 1456-1468. https://doi.org/10.1109/TIFS.2013.2273394

Li, C., & Zhang, J. (2021). Velocity Analysis Using Separated Diffractions for Lunar Penetrating Radar Obtained by Yutu-2 Rover. *Remote Sensing,* 13(7), 1387. https://doi.org/10.3390/rs13071387

Li, C., Lin, Y., Lv, W. M., & Zhang, J. H. (2021). Eliminating above-surface diffractions from GPR data using iterative Stolt migration. *Geophysics,* 86(1), H1-H11. https://doi.org/10.1190/geo2019-0796.1

Lin, P., Peng, S., Cui, X., Du, W., & Li, C. (2022). Effective diffraction separation using the improved optimal rank-reduction method. *Geophysics,* 87(3), V169-V182. https://doi.org/10.1190/geo2021-0326.1

Lin, P., Peng, S., Xiang, Y., Li, C., & Cui, X. (2023). Diffraction imaging of discontinuities using migrated dip-angle gathers. *Geophysics,* 88(1), V21-V32. https://doi.org/10.1190/geo2022-0100.1

Lowney, B., Lokmer, I., O'Brien, G. S., Amy, L., & Lgoe, M. (2020). Enhancing interpretability with diffraction imaging using plane-wave destruction aided by frequency-wavenumber f-k filtering. *Interpretation,* 8(3), T541-T554. https://doi.org/10.1190/INT-2019-0199.1

Moldoveanu-Constantinescu, C., & Sacchi, M. D. (2005). Enhanced resolution in Radon domain using the shifted hyperbola equation. *SEG Technical Program Expanded Abstracts,* 24(1), 2277. https://doi.org/10.1190/1.2148171

Nowak, E. J., & Imhof, M. G. (2006). Amplitude preservation of radon-based multiple-removal filters. *Geophysics,* 71(5), V123-V126. https://doi.org/10.1190/1.2243711

Paulus, C., & Mars, J. I. (2006). New multicomponent filters for geophysical data processing. *IEEE Transactions on Geoscience and Remote Sensing,* 44(8), 2260-2270.

Radon, J. (1986). On the determination of functions from their integral values along certain manifolds. *IEEE Transactions on Medical Imaging,* 5(4), 170-176. https://doi.org/10.1109/TMI.1986.4307775

Sacchi, M. D., & Ulrych, T. J. (1995). High-resolution velocity gathers and offset space reconstruction. *Geophysics,* 60(4), 1169-1177. https://doi.org/10.1190/1.1443845

Stone, D. G. (1987). Applications of spatially variant Fourier transforms. *SEG Technical Program Expanded Abstracts*, 611-613. https://doi.org/10.1190/1.1892034

Storath, M., & Weinmann, A. (2018). Fast median filtering for phase or orientation data. *IEEE Transactions on Pattern Analysis and Machine Intelligence,* 40(3), 639-652. DOI: 10.1109/TPAMI.2017.2692779

Sun, H., Gao, F., & Huang, X. (2023). Time-frequency analysis method of seismic data based on sparse constraints for road detection. *IEEE Transactions on Intelligent Transportation Systems*, 25(3), 1-9. https://doi.org/10.1109/TITS.2023.3299353

Sun, T., & Neuvo, Y. (1994). Detail-preserving median based filters in image processing. *Pattern Recognition Letters,* 15(4), 341-347. https://doi.org/10.1016/0167-8655(94)90082-5

Thorson, R., & Claerbout, J. (1985). Velocity stack and slant stack stochastic inversion. *Geophysics,* 50(12), 2727-2741. https://doi.org/10.1190/1.1441893

Trad, D., Ulrych, T., & Sacchi, M. (2003). Latest views of the sparse Radon transform. *Geophysics,* 68(10), 16-409. https://doi.org/10.1190/1.1543224

Wang, J. H., & Lin, L. D. (1997). Improved median filter using min-max algorithm for image processing. *Electronic Letters*, 33(16), 1362-1363. https://doi.org/10.1049/el:19970945

Yang, F. L., Zhao, C., Wei, Z. R., Sun, H., Li, H. F., Zhao, C., & Luo, H. (2020). Inverse gaussian beam stack imaging in 3D crosswell seismic exploration of deviated wells and its application. Applied Geophysics, 17(5-6), 629-638. https://doi.org/10.1007/s11770-019-0830-x

Zhao, J., Yu, C., Peng, S., & Chen, Z. (2019). Online dictionary learning method for extracting GPR diffractions. *Journal of Geophysics and Engineering,* 16(6), 1116-1123. https://doi.org/10.1093/jge/gxz081

Zhao, W., Forte, E., Fontolan, G., & Pipan, M. (2018). Advanced GPR imaging of sedimentary features: Integrated attribute analysis applied to sand dunes. *Geophysical Journal International,* 213(1), 147-156. https://doi.org/10.1093/gji/ggx541

Zhou, W., & Zhang, D. (1999). Progressive switching median filter for the removal of impulse noise from highly corrupted images. *IEEE Transactions on Circuits and Systems II: Analog and Digital Signal Processing*, 46(1), 78-80. https://doi.org/10.1109/82.749102

Zhu, W., Kelamis, P. G., & Liu, Q. (2004). Linear noise attenuation using local radial trace median filtering. *The Leading Edge,* 23(8), 728-737. https://doi.org/10.1190/1.1786891

Zong, J., Stewart, R. R., & Dyaur, N. (2020). Attenuation of Rock Salt: Ultrasonic Lab Analysis of Gulf of Mexico Coastal Samples. *Journal of Geophysical Research: Solid Earth,* 125(7), e2019JB019025. https://doi.org/10.1029/2019JB019025

Zong, J., Stewart, R. R., Yang, J., Dyaur, N., & Wo, Y. (2023). Investigating seismic mode conversions from an ultra-high-velocity caprock by physical modelling, numerical simulations and a Gulf of Mexico salt proximity VSP survey. *Geophysical Journal International,* 234(2), 1430-1446. https://doi.org/10.1093/gji/ggad151